Journal of Chemistry and Allied Sciences
Volume 1, Issue 1 | 2025 | pp. 41~50
Original Research Article | ***Available online at*** **https://jcasjournal.org/**

SYNTHESIS AND CHARACTERIZATION OF CITRIC ACID-STABILIZED IRON OXIDE NANOPARTICLES FOR BIOMEDICAL APPLICATIONS

Chioma Florence Okafor[1], Bala Anegbe[2]*, Braim Shwana [1], Peter Itoya [2]

[1]Department of Chemistry and Forensics, School of Science and Technology, Nottingham Trent University, Nottingham, United Kingdom
[2]Department of Basic and Industrial Chemistry Western Delta University, Oghara, Delta State, Nigeria

***Article History**: Received May 2025; Revised June 2025; Accepted June 2025; Published online July 2025*

***Corresponding Author**: Dr. Bala Anegbe (bala.anegbe@wdu.edu.ng; **ORCID**: https://orcid.org/0000-0002-8629-9140; **Tel:** +234 813 890 2349)*

Article Information

Citation: Okafor, C. F., Anegbe, B., Shwana, B., & Itoya, P. (2025). Synthesis and Characterization of Citric Acid-Stabilized Iron Oxide Nanoparticles for Biomedical Applications. *Journal of Chemistry and Allied Sciences, 1*(1), 41~50.
DOI: https://doi.org/10.60787/jcas.vol1no1.31

The Official Publication of the Tropical Research and Allied Network (TRANet), Department of Chemistry, *Federal University of Technology, Minna*

Abstract

Iron oxide nanoparticles (MNPs) have emerged as a versatile class of nanomaterials with promising biomedical applications, particularly in targeted drug delivery, imaging, and diagnostics. This study reports the synthesis of iron oxide magnetic nanoparticles via a chemical coprecipitation method, stabilized with citric acid to prevent aggregation and improve colloidal stability. The synthesized nanoparticles were thoroughly characterized using dynamic light scattering (DLS), zeta potential measurements, scanning electron microscopy (SEM), transmission electron microscopy (TEM), Fourier-transform infrared spectroscopy (FTIR), ultraviolet-visible (UV-Vis) spectroscopy, and X-ray diffraction (XRD). The results confirmed the successful synthesis of uniformly sized, spherical iron oxide nanoparticles with high crystallinity and surface stability. This foundational work sets the stage for the incorporation of these MNPs in advanced biomedical systems, including targeted drug delivery.

***Keywords**: Iron oxide nanoparticles; Coprecipitation; Citric acid stabilization; Magnetic nanoparticles; Biomedical applications.*

Graphical Abstract

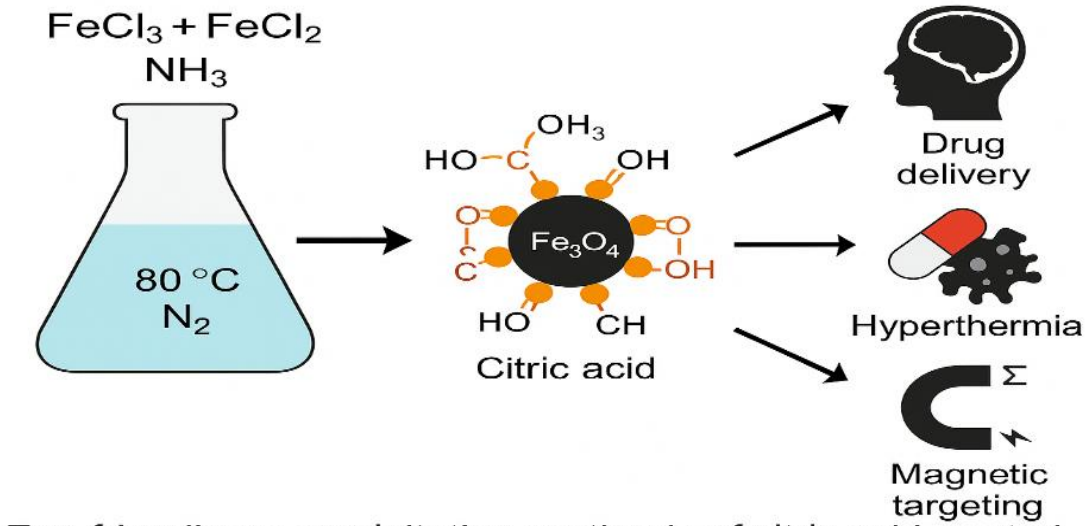

Eco-friendly co-precipitation synthesis of citric acid–coated Fe_3O_4 nanoparticles for potential biomedical use

1.0 INTRODUCTION

Iron oxide nanoparticles (MNPs) have emerged as a critical class of nanomaterials with a broad spectrum of applications across disciplines, including catalysis and photocatalysis, magnetic fluids (ferrofluids), environmental remediation, energy storage, and particularly, biomedical sciences [1–3]. Among these fields, the biomedical applications of iron oxide nanoparticles have garnered the most attention due to their unique combination of physical and chemical properties, making them highly suitable for targeted drug delivery, magnetic resonance imaging (MRI), hyperthermia therapy, magnetofection, and tissue engineering [4–6]. The ability to manipulate these nanoparticles using external magnetic fields, combined with their biocompatibility and nanoscale size, allows for high precision in diagnostics and therapeutics.

Iron oxide nanoparticles, particularly magnetite (Fe_3O_4) and maghemite (γ-Fe_2O_3), are the most widely studied MNPs due to their favorable magnetic properties, relative non-toxicity, and ease of synthesis [4-6]. For biomedical applications, several criteria must be met to ensure functionality and safety. These include chemical stability in physiological environments, particle sizes typically below 100 nm to facilitate cellular uptake, superparamagnetic behavior at body temperature, high magnetic saturation, and a narrow particle size distribution [3, 5]. However, one of the primary challenges lies in ensuring the stability and dispersibility of these nanoparticles in aqueous and physiological solutions. Bare MNPs tend to aggregate and oxidize due to high surface energy and magnetic dipole-dipole interactions, thereby losing their superparamagnetic properties and biocompatibility [7–9].

To overcome these limitations, surface modification is essential. Coating MNPs with biocompatible materials prevents agglomeration, sedimentation, and oxidative degradation while simultaneously improving their colloidal stability and functional versatility [7–9]. Both organic and inorganic materials have been investigated for this purpose, but organic molecules offer greater versatility in tailoring surface chemistry for specific biomedical uses. Among them, citric acid ($C_6H_8O_7$) has recently attracted considerable interest as a stabilizing agent due to its strong chelating ability and exceptional biocompatibility [10]. Citric acid contains three carboxylic acid groups and a hydroxyl group, which allow it to form stable coordination complexes with iron ions on the nanoparticle surface. This not only provides a steric barrier against aggregation but also renders the nanoparticles hydrophilic, enhancing their dispersibility in biological media [11, 12]. Citric acid-coated MNPs have shown great promise in applications such as MRI contrast agents, hyperthermia treatment, drug delivery systems, and biosensors [11, 12].

Moreover, citric acid plays a dual role during nanoparticle synthesis. It influences the nucleation and crystal growth phases, contributing to the formation of uniform, monodisperse nanoparticles [13, 14]. However, the choice of synthesis method remains critical in determining the final properties of the nanoparticles. Several synthetic routes exist, including sol-gel, thermal decomposition, hydrothermal, and co-precipitation techniques [4–6]. Among these, co-precipitation stands out for its simplicity, scalability, and environmental friendliness. It allows for relatively low-temperature synthesis using aqueous precursors and results in nanoparticles with tunable properties by controlling parameters such as pH, temperature, and reagent concentration [5, 6]. Additionally, the reaction by-products of this method, typically nitrogen, water, and carbon dioxide, are environmentally benign, making it a green synthesis approach.

Despite the abundance of literature on MNPs synthesis and stabilization, challenges remain in developing a one-step, eco-friendly method that yields nanoparticles with consistent morphology, high stability, and functional performance in biological systems. In this study, we report the synthesis and characterization of iron oxide nanoparticles stabilized with citric acid via a chemical co-precipitation method. The objective is to obtain biocompatible, monodisperse MNPs with appropriate physicochemical properties for future biomedical applications. By optimizing the synthesis conditions and leveraging citric acid's stabilizing and chelating capabilities, this work aims to contribute to the growing field of nanoparticle-based diagnostic and therapeutic technologies.

2.0 MATERIALS AND METHODS

2.1 Materials

Iron (III) chloride hexahydrate ($FeCl_3 \cdot 6H_2O$), iron (II) chloride tetrahydrate ($FeCl_2 \cdot 4H_2O$), 25% ammonia solution, citric acid, deionized water, and ethanol were purchased from Sigma-Aldrich. All reagents were of analytical grade and used as received.

2.2 Synthesis of Iron Oxide Nanoparticles (MNPs)

The MNPs were synthesized via the conventional chemical co-precipitation method as described by Braim *et al.* [15], with slight modifications. Briefly, ferric chloride hexahydrate ($FeCl_3 \cdot 6H_2O$, 3.65 g, 13.5 mmol) and ferrous chloride tetrahydrate ($FeCl_2 \cdot 4H_2O$, 1.34 g, 6.75 mmol) were dissolved in 10 mL of deionized water in a 100 mL two-neck round-bottom flask. The solution was heated to 80 °C and maintained under a nitrogen atmosphere with constant stirring at 650 rpm for 30 minutes to prevent oxidation of Fe^{2+} ions. Subsequently, 12.5 mL of 25% aqueous ammonia was added dropwise via syringe under the same temperature and inert conditions. This

  | DOI: https://doi.org/10.60787/jcas.vol1no1.31|

resulted in a visible color change from brown to black, indicating the formation of iron oxide nanoparticles. After 30 minutes of additional stirring, citric acid (1.5 g) was introduced as a capping agent to prevent agglomeration of the particles. A 2:1 molar ratio of Fe^{3+} to Fe^{2+} was used to ensure stoichiometric formation of Fe_3O_4, and the citric acid dosage (1.5 g) was optimized based on preliminary trials for maximum stability without excess surface residue.
The mixture was then allowed to cool to room temperature. The black precipitate was magnetically separated, washed three times with deionized water and twice with ethanol to remove residual ions and impurities. The purified nanoparticles were finally air-dried at ambient temperature for 24 hours to yield dried iron oxide nanoparticles.

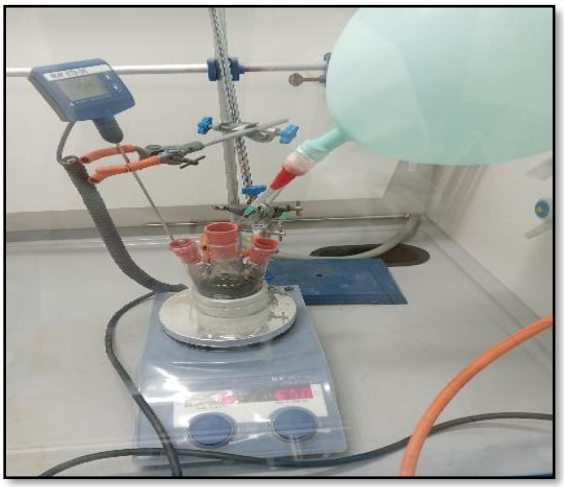

Figure 1: laboratory setup during MNPs synthesis

2.3 Characterization

2.3.1 Dynamic Light Scattering (DLS)

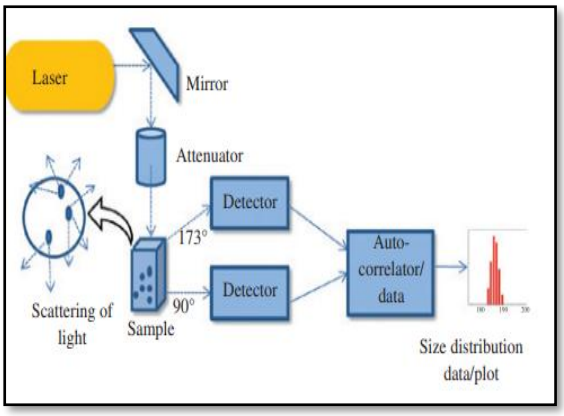

Figure 2: Schematic diagram showing the principle of a DLS [16]

Dynamic Light Scattering (DLS) was employed to evaluate the hydrodynamic diameter, polydispersity index (PDI), and zeta potential of the synthesized iron oxide nanoparticles. DLS measures the intensity of light scattered by particles undergoing Brownian motion, with smaller particles diffusing faster than larger ones [16,17]. The measurements were performed at room temperature using a Nano Plus zeta/nano particle analyser. For hydrodynamic diameter and PDI measurements, 0.015 g of synthesized MNPs was dissolved in 10 mL of distilled water and sonicated for 30 minutes. The resulting suspension was loaded into a 2 mL cuvette using a syringe and analysed following the NickRes Group standard operating procedure (SOP). The zeta potential was measured using the same instrument but with a separate zeta cell. The sonicated nanoparticle suspension was loaded into the zeta cell using a 1 mL syringe. The measurement parameters included a viscosity of 0.890 cP, refractive index of 1.3350, dielectric constant of 78.3, and a repetition count of 1.

2.3.2 Magnetic Properties

To assess the magnetic properties of the synthesized MNPs, an external magnetic field (magnet) was applied. Images were taken before and during magnetic exposure to visually demonstrate the nanoparticles' superparamagnetic-like behaviour or magnetic responsiveness.

2.3.3 Scanning Electron Microscopy (SEM) and Energy Dispersive X-ray Fluorescence Spectrometry (EDS)

The surface morphology and elemental composition of the magnetite nanoparticles were characterized using a SEM (JEOL JSM-7100FLV, Germany) equipped with EDS. SEM utilizes both electrostatic and electromagnetic lenses to produce high-resolution images by scanning the particle surface with an electron beam [16]. Before analysis, the samples were mounted on aluminium stubs with double-sided carbon tape. The stubs were placed in specimen holders and introduced into the chamber. SEM measurements were carried out at an accelerating voltage of 15 kV and a working distance of 10.0 mm. Images were captured at various magnifications using the MALIGN and wobbler alignment tools. Image analysis was performed with ImageJ software. EDS was used to determine the elemental composition of selected SEM image spectra. The analysis was performed at accelerating voltages of 20–30 kV and a working distance of 10.0 mm.

2.3.4 Transmission Electron Microscopy (TEM)

TEM (JEOL 2100 Plus, Germany) was used to examine the morphology and core size of MNPs. TEM projects an electron beam through a thin slice of the sample to generate two-dimensional images [16]. Sample preparation involved dispersing 0.01 g of the nanoparticles in 10 mL of deionized water, followed by 30 minutes of sonication. A 50 µL drop of the suspension was placed on a TEM grid and dried for 15 minutes. The grid was then loaded into the sample holder for analysis. The microscope was

  | DOI: https://doi.org/10.60787/jcas.vol1no1.31|

operated at a current of approximately 5.6 µA and a magnification of 40,000×. Images were captured using the GATPC software, and particle size was calculated using ImageJ software.

2.3.5 FT-IR Spectroscopy

FT-IR spectroscopy was conducted using an Agilent CARY 630 spectrometer (Santa Clara, CA, USA) within a scanning range of 400–4000 cm^{-1}. The aim was to identify functional groups and bond characteristics of the synthesized and modified nanoparticles. No prior sample preparation was required. The diamond sample window and press tip were cleaned with acetone. Background measurements were first taken, after which samples were placed on the crystal surface for scanning. The data was processed using ACD Labs software.

2.3.6 UV-Visible Spectroscopy

A Jasco V-670 spectrometer was used to determine the optical properties of the nanoparticles in the range of 200–800 nm. The absorption profile was used to confirm nanoparticle synthesis and optical behavior.

2.3.7 X-Ray Diffraction, XRD

XRD analysis was carried out using a Rigaku Smartlab X-ray diffractometer (China) to determine the crystalline structure of synthesized and coated nanoparticles. XRD operates on the principle of constructive interference between incident X-rays and the crystalline sample, producing a diffraction pattern unique to each material. Prior to analysis, nanoparticle powders were finely ground and loaded onto polyethylene XRD plates. The analysis was performed at a tube voltage of 40 kV and current of 50 mA. The diffraction patterns were recorded across a 2θ range and used to confirm crystallinity.

3.0 RESULTS AND DISCUSSION

3.1 Visual Observation and Magnetic Properties

The nanoparticles synthesized via chemical coprecipitation method were black in colour, suggesting the formation of iron oxide. When brought close to a magnet the nanoparticles were attracted towards it as seen in Figure 3 and returned to their non-magnetic state on removal of the magnet confirming magnetic responsiveness.

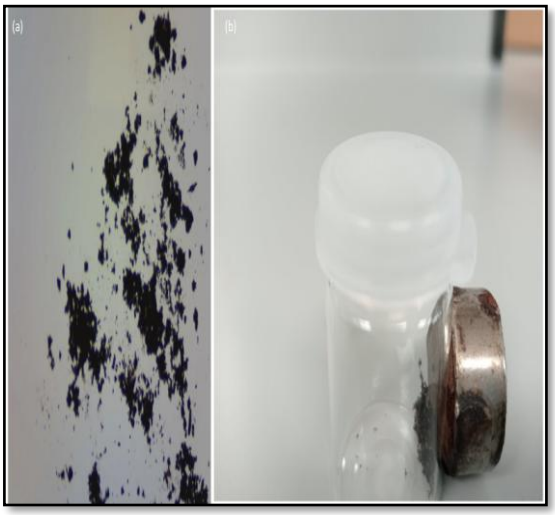

Figure 3: Images of the synthesized iron nanoparticles

3.2 Particle Size Distribution and Surface Charge Analysis

The dynamic light scattering analysis data (Figure 4) revealed an average hydrodynamic size of 171.1 ± 76.8 nm, which exceeds the ideal range (<100 nm) for biomedical uptake. This is likely due to agglomeration and hydration shell formation in aqueous medium, as TEM results (below) show a much smaller core size. The PDI of 0.138 indicates a narrow size distribution, suitable for biomedical use. Zeta potential was measured as –36.01 mV, which is more negative than –30 mV, confirming good colloidal stability [18]. Values more negative than –30 mV typically reflect strong electrostatic repulsion between particles.

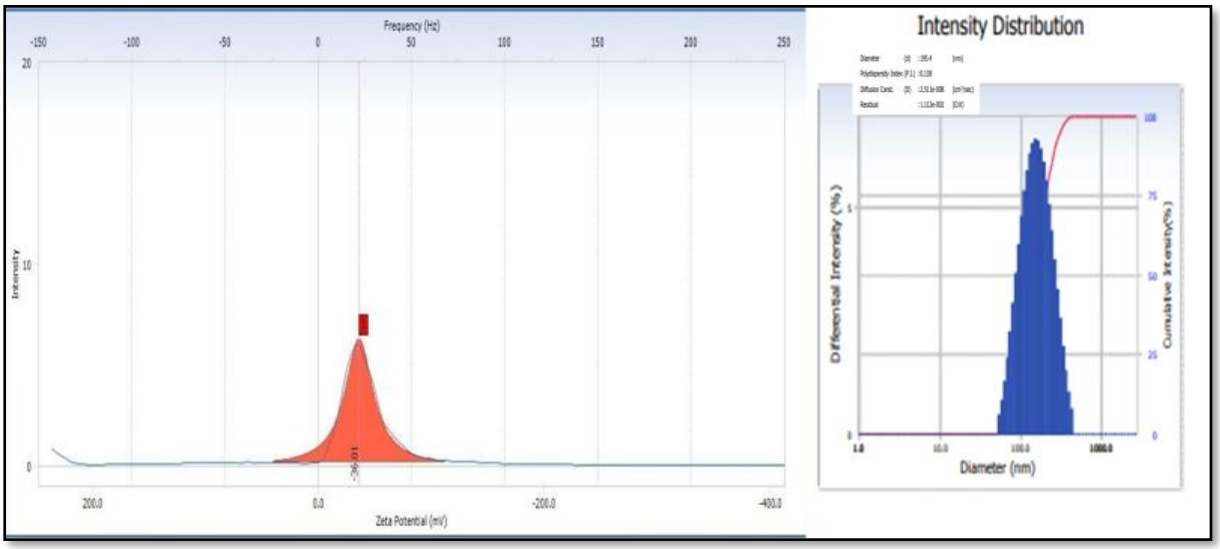

Figure 4: DLS size and Zeta Potential data for the iron oxide nanoparticles

  | DOI: https://doi.org/10.60787/jcas.vol1no1.31| CC BY 4.0

Table 1: DLS Data for the Synthesized iron oxide nanoparticles

Compound	Average Diameter (nm)	PDI	Zeta potential (mV)
Synthesized MNPs	171.1 ± 76.8	0.138	36.01

3.3 Morphology Analysis by SEM and TEM

The SEM images (Figure 5) of the MNPs at varying magnifications showed images that are spherical in shape with different sizes from 1 µm to 100 nm. This indicates that some of the particles are aggregated because of the magnetic properties of the nanoparticles. When compared with the average diameter from DLS, this suggests that the measured value might be because of aggregated particles rather than individual particles.

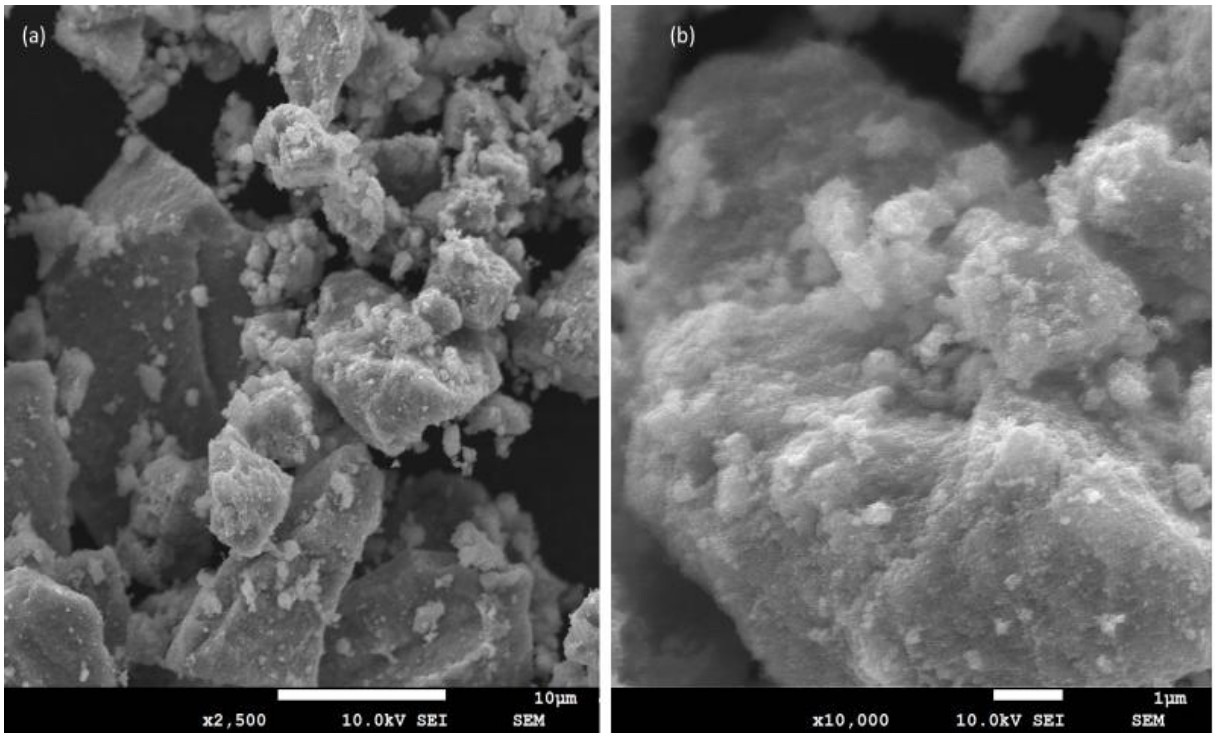

Figure 5a: SEM Images of the Synthesized iron oxide nanoparticles at varying magnification values (a & b)

  | DOI: https://doi.org/10.60787/jcas.vol1no1.31|

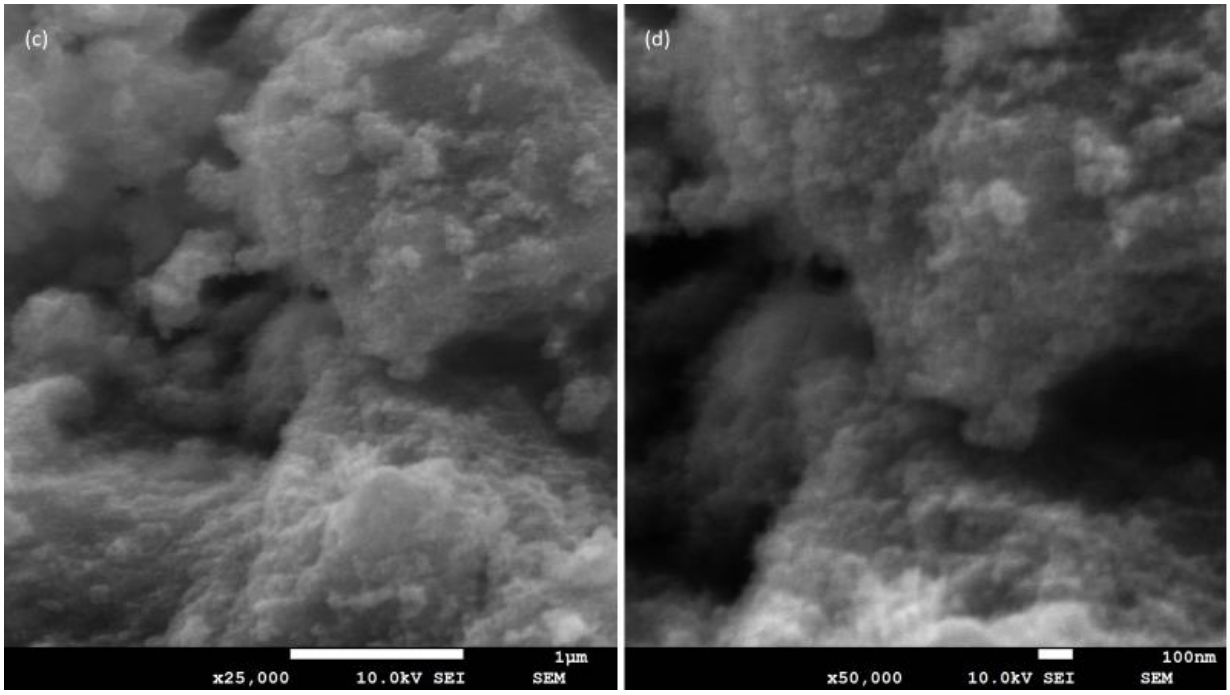

Figure 5b: SEM Images of the Synthesized iron oxide nanoparticles at varying magnification values (c & d)

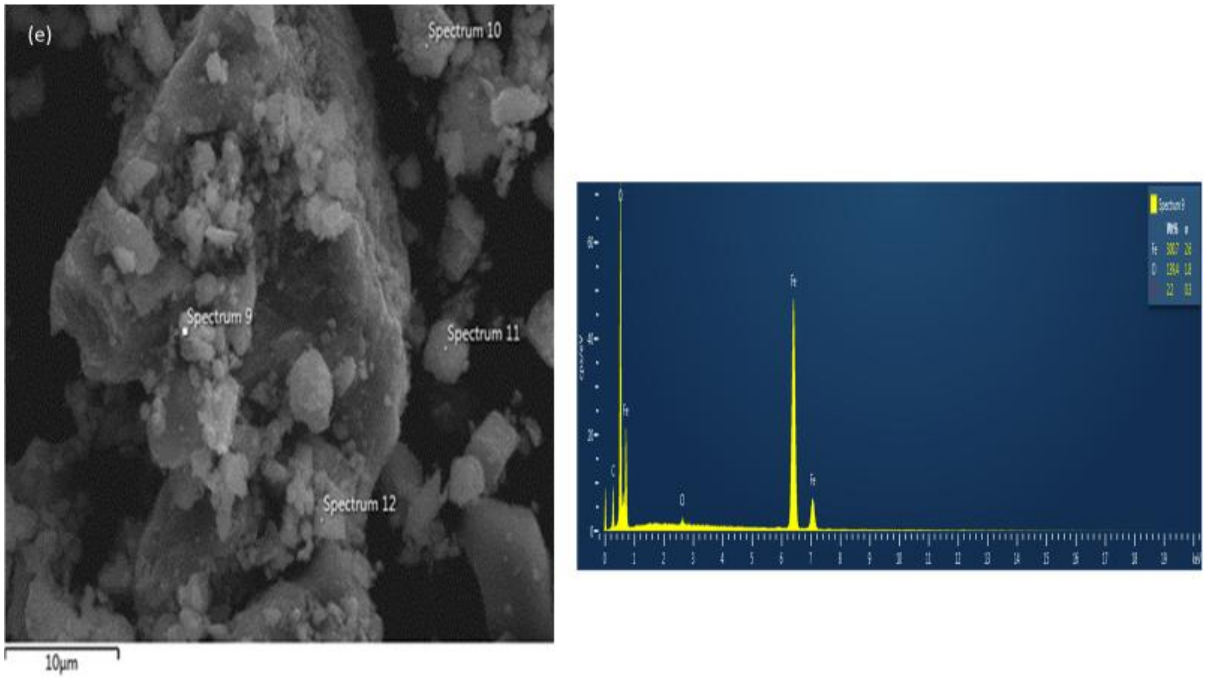

Figure 5c: SEM Images of the Synthesized iron oxide nanoparticles and EDS Mapping (e)

Transmission electron microscopy (TEM) determines the size and shape of the nanoparticles and gives insight on their morphology. The images (Figure 6) showed the formation of spherical shaped nanoparticles with an average size of 7.04 ± 1.71 nm. Though there were few large particles due to the aggregation of smaller particles, the majority of the particles in the TEM images were less than 20nm, indicating that they are superparamagnetic. This further confirms the suitability of the synthesized nanoparticles for anticancer drug delivery systems [19-21].

  DOI: https://doi.org/10.60787/jcas.vol1no1.31|

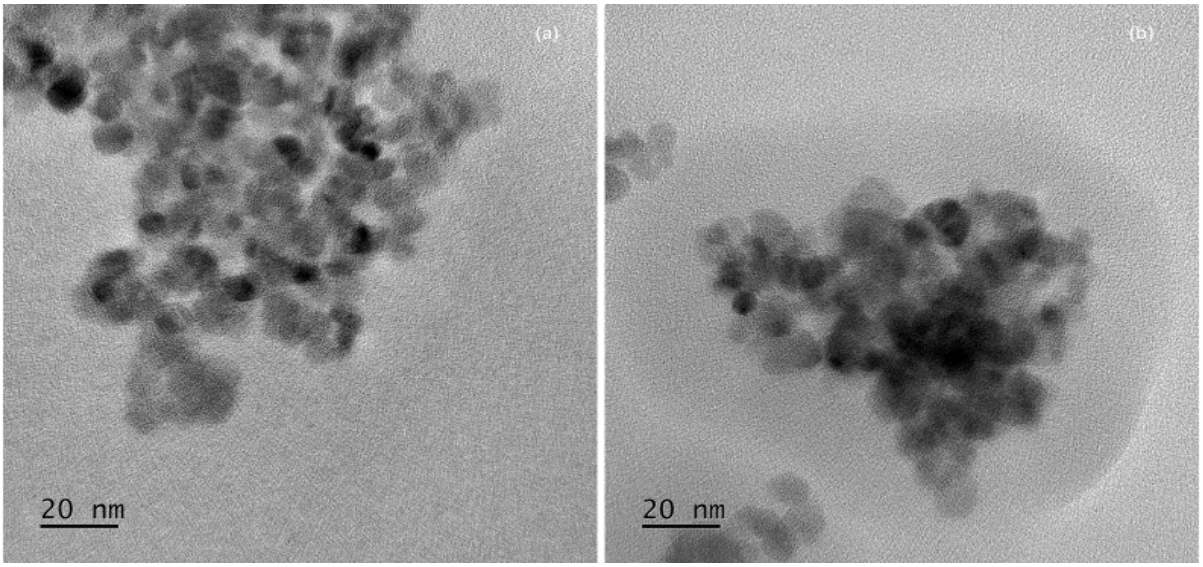

Figure 6: TEM Images of the synthesized iron nanoparticles

3.4 FTIR Spectroscopy

The FT-IR analysis was also used in the characterization of the synthesized MNPs to ascertain the bond-level and the functional groups. The spectrum (Figure 7) of the prepared iron oxide nanoparticles exhibited defined peaks at 552, 1060, 1559, 2952, and 3130 cm^{-1}. The peak at 552 cm^{-1} fell within the fingerprint region of metal-oxygen bond, in this case, Fe-O bond, which further confirms that the developed nanoparticles were iron oxide [22]. The peak at 1060 cm^{-1} likely corresponds to C–O stretching vibrations from citrate groups bound to the nanoparticle surface, while the peak at 1394 cm^{-1} indicates the presence of an O-H bending, attributed to the citric acid used as a capping agent to minimise aggregation. The broad peak between 2952 and 3130 cm^{-1} is attributed to O–H stretching vibrations, likely from surface-bound hydroxyl groups and adsorbed water. These results were consistent with the SEM-EDX mapping analysis (Figure 5e) which showed the elemental composition at various spectrum of the SEM images to be mostly Fe and O. The findings agree with those of Frounchi and Shamshiri [20], as well as other studies using hydrothermal synthesis methods [23, 24].

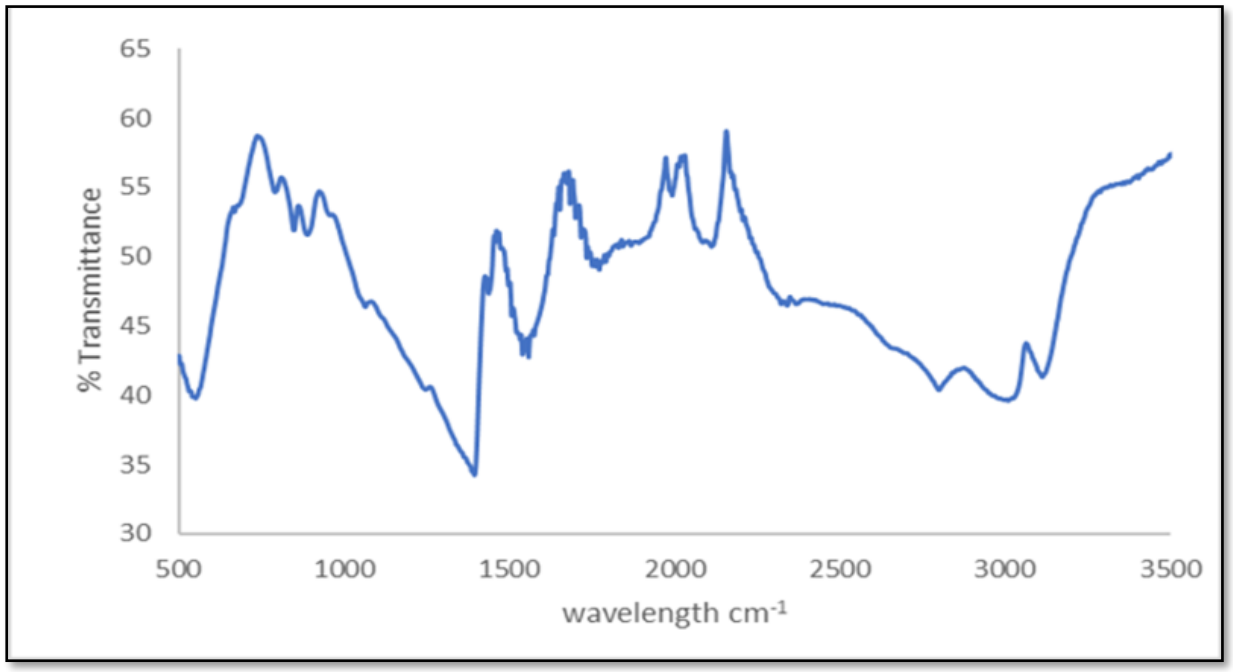

Figure 7: FT-IR Spectrum of the iron nanoparticles

  DOI: https://doi.org/10.60787/jcas.vol1no1.31|

3.5 UV-Visible Spectroscopy

The UV-Visible spectrum (Figure 8) of the powdered iron oxide nanoparticles showed a broad peak between 400 – 600 nm. From other studies, an absorption peak in the wavelength range of 400-600 nm defines the characteristic of iron oxide nanoparticles [22, 25]. This is in good agreement with the characteristic FT-IR peak at 552 cm^{-1} for Fe-O bond.

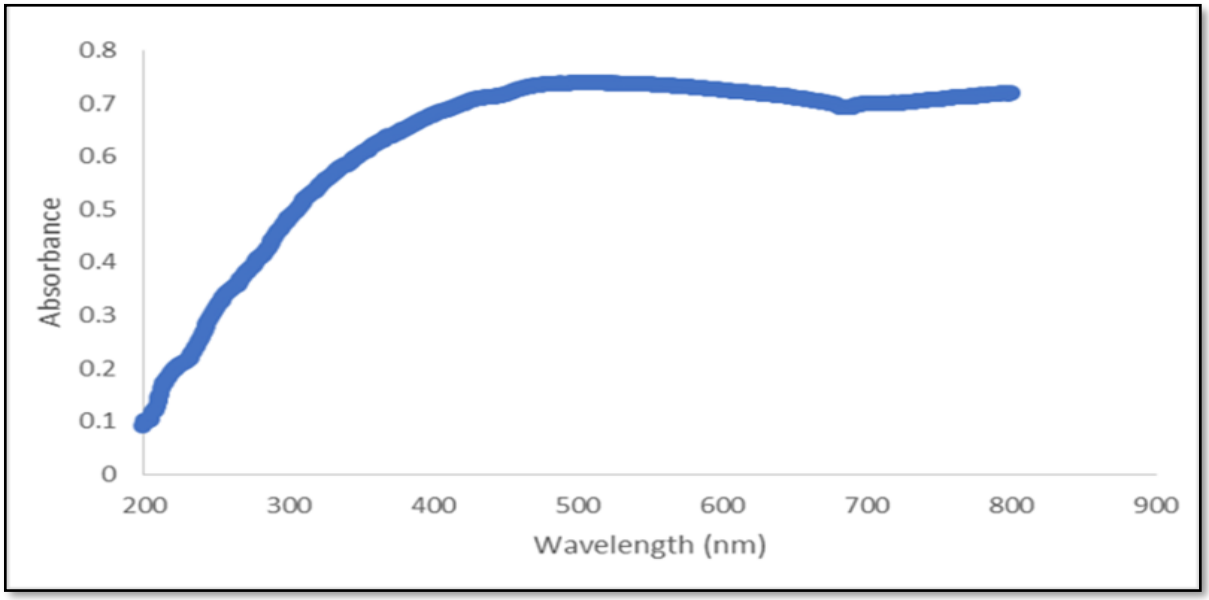

Figure 8: UV-Visible Spectrum of the iron nanoparticles

3.6 X-Ray Diffraction (XRD) Analysis

Finally, the XRD study was used to assess the structure and crystallinity of the synthesized nanoparticles. From the XRD spectrum (Figure 9), peaks detected were 35.56°, 56.9° and 62.60° at 2θ range. The conspicuous peak at 35.56° confirms the formation of an iron oxide nanoparticle, which agrees with Jones *et al.* [19] that standard diffraction peaks of magnetite and maghemite are 35.43° and 35.62° respectively. In addition, the peak pattern was identical to the Bragg reflections of the spinel ferrite structure [26, 27].

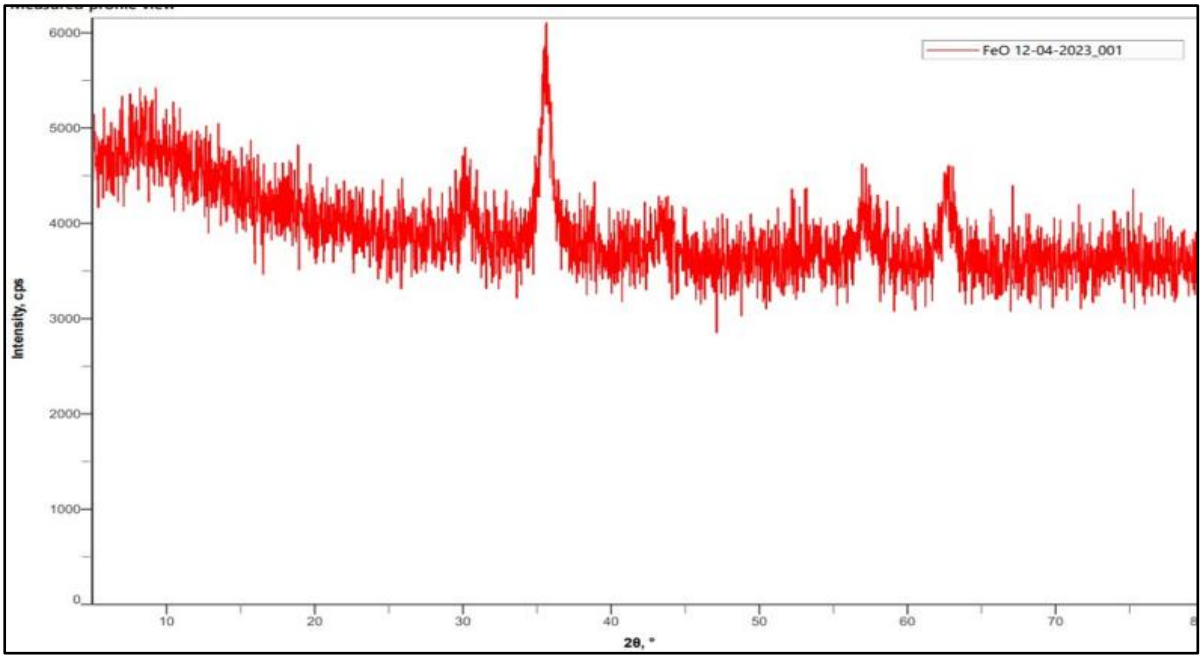

Figure 9: XRD Spectrum of the iron nanoparticles

 DOI: https://doi.org/10.60787/jcas.vol1no1.31|

4.0 CONCLUSION

Citric acid-stabilized iron oxide nanoparticles were successfully synthesized using a green co-precipitation approach. The particles exhibited superparamagnetic-like core sizes (<20 nm by TEM), good dispersibility (zeta potential of –36.01 mV), and strong Fe–O bonding as shown by FTIR and XRD. While TEM confirmed their suitability for biomedical use, DLS revealed larger hydrodynamic sizes due to aggregation or surface hydration. The magnetic behavior was only qualitatively demonstrated; thus, further magnetic characterization using vibrating sample magnetometer (VSM) or superconducting quantum interference device (SQUID) is needed to determine superparamagnetic properties. This study provides a sustainable and reproducible method for producing biocompatible MNPs and lays the groundwork for future functionalization studies in nanomedicine, environmental remediation, and smart materials.

Conflict of Interest

The authors declare that they have no conflicts of interest.

Data Availability Statement

The datasets generated and/or analyzed during the current study are available from the corresponding author on reasonable request.

Authors' Contribution

Okafor C. F. conducted the experiments and generated the data. Shwana B. acquired funding, supervised the original work, and contributed to the conceptualization and methodology. Anegbe B. and Itoya P. were responsible for drafting the original manuscript, as well as reviewing and editing it. Okafor C. F. and Itoya P. also contributed to data analysis and interpretation.

Authors' Declaration

The authors confirm that this work is original, has not been published previously, and is not under consideration by any other journal. They accept full responsibility for the integrity of the data and the accuracy of the reported findings, and will accept all liability for any claims arising from the content.

Ethical Declarations Human/Animal Studies

This research did not involve the use of human participants or animal subjects.

Acknowledgments

The authors gratefully acknowledge the Department of Chemistry and Forensics, School of Science and Technology, Nottingham Trent University, Nottingham, United Kingdom, for providing the research facilities and enabling environment for this work. Special appreciation is extended to the dedicated laboratory staff for their technical assistance and valuable contributions during experimental procedures. The authors also thank the Shwana Lab team for their expertise in sample preparation and equipment maintenance. Finally, they express gratitude to colleagues and researchers whose insightful discussions helped refine this study.

REFERENCES

[1] Lu, A. H., Salabas, E. L., & Schüth, F. (2007). Magnetic nanoparticles: Synthesis, protection, functionalization and application. *Angewandte Chemie International Edition*, 46(8), 1222–1244. https://doi.org/10.1002/anie.200602866

[2] Ianoș, R., Păcurariu, C., Muntean, S. G., Muntean, E., Nistor, M. A., & Nižňanský, D. (2018). Combustion synthesis of iron oxide/carbon nanocomposites, efficient adsorbents for anionic and cationic dyes removal from wastewaters. *Journal of Alloys and Compounds*, 741, 1235–1246. https://doi.org/10.1016/j.jallcom.2018.01.240

[3] Păcurariu, C., Paşka, O., Ianoș, R., & Muntean, S. G. (2016). Effective removal of methylene blue from aqueous solution using a new magnetic iron oxide nanosorbent prepared by combustion synthesis. *Clean Technologies and Environmental Policy*, 18(3), 705–715. https://doi.org/10.1007/s10098-015-1041-7

[4] Abu-Noqta, O., Aziz, A., & Usman, A. (2019). Colloidal stability of iron oxide nanoparticles coated with different capping agents. *Materials Today: Proceedings*, 17, 1072–1077. https://doi.org/10.1016/j.matpr.2019.06.106

[5] Alzoubi, F. Y., Abu Noqta, O., Al Zoubi, T., Al-Khateeb, H. M., Alqadi, M. K., Abuelsamen, A., Makhadmeh, G. N. (2023). A novel one-pot synthesis of PVP-coated iron oxide nanoparticles as biocompatible contrast agents for enhanced T2-weighted MRI. *Journal of Composites Science*, 7(3), 131. https://doi.org/10.3390/jcs7030131

[6] Al Zoubi, T., Albiss, B., Al-Akhras, M.-A., Qutaish, H., Alabed, E., & Nazrul, S. (2019). NiO nanofillers embedded in graphite/PVA-polymer matrix for efficient electromagnetic radiation shielding. *AIP Conference Proceedings*, 2083(1), 020002. https://doi.org/10.1063/1.5094305

[7] Petcharoen, K., & Sirivat, A. (2012). Synthesis and characterization of magnetite nanoparticles via the chemical co-precipitation method. *Materials Science and Engineering B: Solid-State Materials for Advanced Technology*, 177(5), 421–427. https://doi.org/10.1016/j.mseb.2012.01.003

[8] Benyoucef, M., Usman, M. A. U., Alzoubi, T., & Reithmaier, J. P. (2012). Pre-patterned silicon substrates for the growth of III–V nanostructures. *Physica Status Solidi A*, 209(8), 1579–1583. https://doi.org/10.1002/pssa.201127513

[9] Al-Fandi, M., Oweis, R. J., Albiss, B. A., Alzoubi, T., Al-Akhras, M., Qutaish, H., Khwailah, H., Al-Hattami, S., Al-Shawwa, E. (2015). A prototype ultraviolet light sensor based on ZnO nanoparticles/graphene oxide nanocomposite using low temperature hydrothermal method. *IOP Conference Series: Materials Science and Engineering*, 92, 012038. https://doi.org/10.1088/1757-899X/92/1/012038

[10] Osuna, Y., Gregorio-Jauregui, K. M., Gaona-Lozano, J. G., de la Garza-Rodríguez, I. M., Ilyna, A., Barriga-Castro, E. D., Saade, H., López, R. G. (2012). Chitosan-coated magnetic nanoparticles with low chitosan content

  DOI: https://doi.org/10.60787/jcas.vol1no1.31|

prepared in one-step. *Journal of Nanomaterials*, 2012, 327562. https://doi.org/10.1155/2012/327562

[11] Snoderly, H. T., Freshwater, K. A., Martinez de la Torre, C., Panchal, D. M., Vito, J. N., & Bennewitz, M. F. (2022). PEGylation of metal oxide nanoparticles modulates neutrophil extracellular trap formation. *Biosensors*, 12(2), 123. https://doi.org/10.3390/bios12020123

[12] Cho, M., Villanova, J., Ines, D. M., Chen, J., Lee, S. S., Xiao, Z., Guo, X., Dunn, J. A., Stueber, D. D., Decuzzi, P., & Colvin, V. L. (2023). Sensitive T2 MRI contrast agents from the rational design of iron oxide nanoparticle surface coatings. *The Journal of Physical Chemistry C*, 127(2), 1057–1070. https://doi.org/10.1021/acs.jpcc.2c05390

[13] Wan, J., Jiang, X., Li, H., & Chen, K. (2012). Facile synthesis of zinc ferrite nanoparticles as non-lanthanide T1 MRI contrast agents. *Journal of Materials Chemistry*, 22(27), 13500–13505. https://doi.org/10.1039/C2JM30684K

[14] Benyoucef, M., Alzoubi, T., Reithmaier, J. P., Wu, M., & Trampert, A. (2014). Nanostructured hybrid material based on highly mismatched III–V nanocrystals fully embedded in silicon. *Physica Status Solidi A*, 211(1), 211–215. https://doi.org/10.1002/pssa.201330214

[15] Braim, S. A., Shakesheff, K. M., Saunders, B. R., & Alexander, C. (2016). Biocompatible polymer-coated magnetic nanoparticles for biomedical use. *Journal of Materials Chemistry B*, 4(5), 962–972. https://doi.org/10.1039/C5TB01958F

[16] Hammad, M., Hardt, S., Mues, B., Salamon, S., Landers, J., Slabu, I., Wende, H., Schulz, C., & Wiggers, H. (2020). Characterization of flame-made magnetic iron oxide nanoparticles. *Journal of Alloys and Compounds*, 824, 153814. https://doi.org/10.1016/j.jallcom.2020.153814

[17] Gumustas, M., Sengel-Turk, C. T., Gumustas, A., Ozkan, S. A., & Uslu, B. (2017). Multifunctional systems for combined delivery, biosensing and diagnostics. In A. M. Grumezescu (Ed.), *Multifunctional Systems for Combined Delivery, Biosensing and Diagnostics* (pp. 69–108). Elsevier. https://doi.org/10.1016/B978-0-323-55725-5.00005-8

[18] Nayan, M. B., Jagadish, K., Abhilash, M. R., Namratha, K., & Srikantaswamy, S. (2019). Green synthesis of iron oxide nanoparticles for water treatment applications. *Journal of Water Resource and Protection*, 11(3), 357–370. https://doi.org/10.4236/jwarp.2019.113021

[19] Jones, J. A., Novo, N., Flagler, K., Pagnucco, C. D., Carew, S., Cheong, C., Kong, X. Z., Burke, N. A. D., & Stöver, H. D. H. (2005). Thermoresponsive polymers and their biomedical applications. *Journal of Polymer Science Part A: Polymer Chemistry*, 43(24), 6095–6104. https://doi.org/10.1002/pola.21041

[20] Frounchi, M., & Shamshiri, S. (2015). Synthesis and characterization of thermoresponsive magnetic hydrogels for drug delivery. *Journal of Biomedical Materials Research Part A*, 103(6), 1893–1898. https://doi.org/10.1002/jbm.a.35336

[21] Yang, J., Zou, P., Yang, L., Cao, J., Sun, Y., Han, D., Yang, S., Wang, Z., Chen, G., Wang, B., & Kong, X. (2014). Surface modification of magnetic nanoparticles for targeted drug delivery. *Applied Surface Science*, 303, 425–432. https://doi.org/10.1016/j.apsusc.2014.02.135

[22] Gubin, S. P. (2009). Magnetic nanoparticles: Introduction. In S. P. Gubin (Ed.), *Magnetic Nanoparticles* (pp. 1–9). Wiley-VCH. ISBN: 978-3-527-40790-2

[23] Omwoyo, W. N., Ogutu, B., Oloo, F., Swai, H., Kalombo, L., Melariri, P., Mahanga, G. M., & Gathirwa, J. W. (2014). Development and characterization of a liposomal nanocarrier for antimalarial drug delivery. *International Journal of Nanomedicine*, 9, 3865–3874. https://doi.org/10.2147/IJN.S64018

[24] Obireddy, S. R., Chintha, M., Kashayi, C. R., Venkata, K. R. K. S., & Subbarao, S. M. C. (2020). Biopolymer-based magnetic nanocomposites for environmental and biomedical applications. *ChemistrySelect*, 5(33), 10276–10284. https://doi.org/10.1002/slct.202002605

[25] Park, J., Yu, M. K., Jeong, Y. Y., Kim, J. W., Lee, K., Phan, V. N., & Jon, S. (2009). Antibiofouling polymer-coated superparamagnetic iron oxide nanoparticles for hepatoma-targeted imaging and therapy. *Journal of Materials Chemistry*, 19(41), 6412–6417. https://doi.org/10.1039/B904546A

[26] Yun, S. Y., Lee, J. Y., & Kim, J. (2020). Synthesis and characterization of Fe_3O_4 nanoparticles for biomedical applications. *Korean Journal of Chemical Engineering*, 37(5), 875–882. https://doi.org/10.1007/s11814-020-0494-2

[27] Hammad, M., Hardt, S., Mues, B., Salamon, S., Landers, J., Slabu, I., Wende, H., Schulz, C., & Wiggers, H. (2020). Characterization of flame-made magnetic iron oxide nanoparticles. *Journal of Alloys and Compounds*, 824, 153814. https://doi.org/10.1016/j.jallcom.2020.153814.

  DOI: https://doi.org/10.60787/jcas.vol1no1.31|